Inorganic Chemistry

Article

pubs.acs.org/IC

Neutron Diffraction Study of the Type I Clathrate $Ba_8Al_xSi_{46-x}$: Site Occupancies, Cage Volumes, and the Interaction between the Guest and the Host Framework

John H. Roudebush,[†] Clarina de la Cruz,[‡] Bryan C. Chakoumakos,[‡] and Susan M. Kauzlarich*[,†]

[†]Department of Chemistry, University of California, One Shields Avenue, Davis, California 95616, United States

[‡]Neutron Scattering Science Division, Oak Ridge National Laboratory, Oak Ridge, Tennessee 37831, United States

Supporting Information

ABSTRACT: Samples with the type I clathrate structure and composition $Ba_8Al_xSi_{46-x}$, where x = 8, 10, 12, 14, and 15, were examined by neutron powder diffraction at 35 K. The clathrate type I structure contains Ba cations as guests in a framework derived from tetrahedrally coordinated Al/Si atoms. The framework is made up of five- and six-membered rings that form dodecahedral and tetrakaidecahedral cages. The change in distances between tetrahedral sites across the series is used to develop a model for the mixed Al/Si occupancy observed in the framework. The calculated volumes of the cages that contain the Ba atoms display a linear increase with increasing Al composition. In the smaller dodecahedral cages, the Ba atomic displacement parameter is symmetry constrained to be isotropic for all compositions. In the larger tetrakaidecahedral cages, the anisotropic atomic displacement of the Ba atom depends upon the composition: the displacement is perpendicular (x = 8) and parallel (x = 15) to the six-membered ring. This difference in direction of the displacement parameter is attributed to interaction with the Al in the framework and not to the size of the cage volume as x increases from 8 to 15. The influence of the site occupation of Al in the framework on displacement of the cation at the 6*d* site is demonstrated.

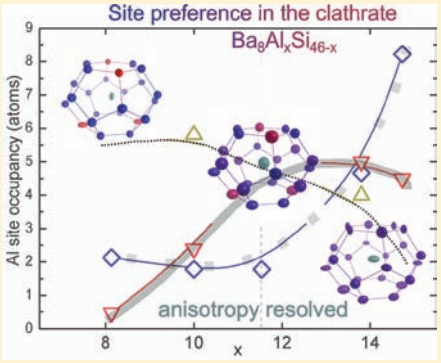

INTRODUCTION

Inorganic clathrate structured compounds are of interest because they have demonstrated superconductivity,[1] hydrogen storage capability,[2] and good thermoelectric properties.[3,4] In the area of thermoelectrics, the type I clathrate structure is of interest for its favorable electronic transport and thermal conductivity properties: The most widely studied is the $Ba_8Ga_{16}Ge_{30}$ composition.[4−11] Isoelectronic clathrate structures with Al and Si frameworks have been studied far less, although a high efficiency thermoelectric made from Al and Si would be desirable from an economic and weight perspective.[12−14]

The intermetallic type I clathrate structure (Figure 1a, space group $Pm\bar{3}n$) consists of a framework of 4-coordinate atoms encapsulating a larger guest atom. The framework atoms form cages of different sizes: a dodecahedron (Wyckoff site 2*a*) and a tetrakaidecahedron (Wyckoff site 6*d*). The cages are formed from three different framework sites (distinguished by symmetry, named by their Wyckoff positions): 24*k*, 16*i*, and 6*c*.

Each site has a unique connectivity to the other framework sites (Figure 1). The 24*k* site is connected to one 24*k* site, two 16*i* sites, and one 6*c* site. The 16*i* site is connected to three 24*k* sites and one 16*i* site. The 6*c* site is connected to four 24*k* sites. As a consequence of the site connectivity, the four discrete bonds in the structure correspond to the distances between various sites: 16*i*−16*i*, 16*i*−24*k*, 24*k*−24*k*, and 24*k*−6*c*. Additionally, because of this site connectivity, a systematic lengthening of the distances between sites is expected when Si is replaced by Al, corresponding to the following: (1) Substitution on the 16*i* site should increase the 16*i*−16*i* and 16*i*−24*k* distances but in a 1:3 ratio due to their site connectivity; (2) replacement at the 24*k* site should increase

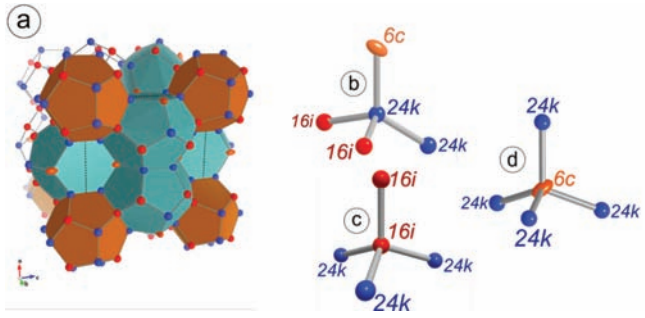

Figure 1. (a) Crystal structure of the type I clathrate showing the large tetrakaidecahedral (blue) and smaller dodecahedral (brown) cages. Local geometry and connectivity of the framework sites (b) 24*k*, (c) 16*i*, and (d) 6*c* determined from the refinement of NPD data for $Ba_8Al_8Si_{38}$ at 35 K. Framework sites are identified by their Wyckoff symbols and represented as thermal ellipsoids (99% probability): 24*k* (blue), 16*i* (red), and 6*c* (yellow).

Received: September 26, 2011
Published: December 22, 2011

   dx.doi.org/10.1021/ic202095e | *Inorg. Chem.* 2012, 51, 1805−1812

the 16*i*−24*k*, 24*k*−24*k*, and 24*k*−6*c* distances in a 1:2:1 ratio; and (3) replacement of Si for Al at the 6*c* site should only increase the 24*k*−6*c* distance.

The chemical flexibility of the type I clathrate structure is what makes it a rich area of study but also a complex one. A sensitive connection between framework composition and properties has been demonstrated.[7,9,15] Common to all type I clathrates are their low thermal conductivity. For example, the thermal conductivity of $Ba_8Al_{15}Si_{31}$[14] is an order of magnitude lower than that of silicon, and for some compositions, the thermal conductivity displays "glasslike" behavior.[5,7] Changes in thermal conductivity were first attributed to the magnitude of the displacement of the guest cation in the large cage, that is, the cation on the 6*d* site in the center of the tetrakaidecahedron. Phases with small cations or large cages such as $Sr_8Ga_{16}Ge_{30}$,[16] $Eu_8Ga_{16}Ge_{30}$,[17] and $Ba_8Ga_{16}Sn_{30}$[18] have exceptionally low thermal conductivity and display glasslike behavior. These observations lead researchers to focus on lowering thermal conductivity by maximizing the space in which the cation at the 6*d* site can "rattle". However, the relation between thermal conductivity and structure has proven to be more complex. A study, by way of neutron diffraction, on the thermal conductivity in *n* type and *p* type $Ba_8Ga_{16}Ge_{30}$ found that the *p* type phase displays glasslike thermal conductivity, while the *n* type does not.[7] This difference in thermal conductivity was surprising because it could not be explained by composition; instead, the authors pointed to a subtle difference in site occupancies between the *n* and the *p* type samples. A second study on $Ba_8Al_{16}Ge_{30}$, this time with a focus on synthesis methods, also demonstrated that subtle differences in framework occupancies affect the guest cation displacement parameter, thereby impacting the thermoelectric properties.[16,19] Specifically, the $Ba_8Al_{16}Ge_{30}$ study showed that in samples with fewer Al atoms at the 6*c* framework site, an increase in the displacement of the Ba at the 6*d* site is observed. The idea that the framework occupancies play a role in the displacement of the guest cations is widely stated in the literature, but because of concurrent differences in cage volume between compositions, it is difficult to determine which plays a larger role in influencing the displacement: cage volume or site occupancies?

$Ba_8Al_xSi_{46-x}$ is a good candidate to resolve this debate. First, the solid solution has a large phase range, $8 \leq x \leq 15$ with no vacancies. Second, the largest observed lattice parameter (x = 15) is smaller than both that of $Ba_8Ga_{16}Ge_{30}$ and $Ba_8Al_{16}Ge_{30}$, thereby shortening the distance between guest and framework and eliminating the possibility that large displacements are due to a large cage volume.

In this study, neutron powder diffraction (NPD) is used to probe mixed Al/Si occupancy in the clathrate type I structure corresponding to the following formula $Ba_8Al_xSi_{46-x}$ (x = 8, 10, 12, 14, and 15). With X-rays, the similar values of Z for Al and Si (Z^2 ratio: 196/169 = 1.16) make site occupancy refinement difficult. The contrast for neutron diffraction is slightly better; the neutron scattering length ratio of Al to Si is 4.15^2 fm/3.45^2 fm = 1.45, and the scattering length of Ba (5.07 fm) is similar.[20] Despite the improvement in contrast between Al and Si with respect to neutron diffraction, direct Rietveld refinement of the site occupancies was not possible due to the limited *Q*-range of the data. Instead, a site occupancy model was determined by monitoring the distances between Wyckoff sites and assigning increases in distance to the increasing amount of Al.[14] These changes in distances as a function of Al content are used to propose a site occupancy model for each composition. Six possible occupancy models are proposed and refined. Their agreement values, determined by NPD at each composition, are compared. Providing a detailed description of how the group 13 element site substitution depends on x, along with the effect on the displacement parameter, may provide insight into the differences in properties for group 13/14 clathrates as well as providing a strategy when considering incorporation of additional atoms into the framework.

EXPERIMENTAL SECTION

Synthesis. Barium (Sigma Aldrich, 99.99%, dendritic) and aluminum (Sigma-Aldrich, 99.999+%) were used as received and weighed in an argon-filled glovebox with less than 1 ppm of water. Silicon pieces (Alfa Aesar, 99.99999%) were weighed under ambient conditions. Samples with starting ratios 8.1Ba:*X*Al:46-*X*Si (X = 8, 10, 12, 14, and 16) were arc melted on a cooled copper hearth to obtain a button with mass between 1 and 1.5 g and a diameter of ∼1 cm. Mass loss after arc melting was typically between 1 and 2% of the theoretical yield. Samples were placed in alumina crucibles and sealed in a fused silica jacket under vacuum. The X = 8, 10, and 12 samples were annealed at 1020 K, the X = 14 was annealed at 1173 K, and the X = 16 was annealed at 1273 K. All samples were annealed for 72 h followed by quenching in water. To obtain the approximately 5 g of sample necessary for neutron diffraction, phase pure samples with similar lattice parameters ($\Delta a \leq 0.0001$ Å, determined by powder X-ray diffraction) were combined and mixed using a mechanical ball mill (SPEX 8000D Mixer Mill) for 5 min in a steel container with tungsten carbide end caps.

Powder X-ray Diffraction. Powder diffraction patterns were collected from 10 to 90° 2θ on a Bruker D8 Advance diffractometer employing Cu Kα radiation at 40 KeV and 40 mA.

Electron Microprobe Analysis. Small amounts (∼50 mg) of powder from each sample batch were mounted in epoxy and polished for analysis on a Cameca SX-100 electron microprobe equipped with five wavelength dispersive spectrometers. The standards $BaAl_{3.54}Si_{0.41}$, Al, and Si were used for Ba, Al, and Si, respectively. The instrument was operated at an accelerating voltage of 10 keV and current of 10 nA. Data were collected in a series of points at least 5 μm apart, and weight percentage totals were 100(1)%, indicating that Ba, Al, and Si are the only elements detectable within the instrumental conditions. Atomic percentages were used to calculate nominal compositions.

NPD. NPD measurements were performed at the HB2a high-resolution neutron powder diffractometer located at the High Flux Isotope Reactor at Oak Ridge National Laboratory (ORNL). Powdered samples were loaded in vanadium cans and installed on a top-loading low-temperature cryostat. Data were collected at 35 K using the 1.5385 Å wavelength, produced by a Ge [115] monochromator and 12′-21′-6′ collimation, that is, 12′ Soller collimator before the monochromator, 21′ Soller collimator before the sample, and 6′ Soller collimators before the detectors. For each sample, a data set was collected at 35, 100, 200, 300, 450, and 590 K. The X = 8 sample was measured at 310 K instead of 300 K. For samples X = 12, 14, and 16, an additional data set was measured at 530 K. The focus of this work is the 35 K data set; the temperature-dependent data, along with the corresponding thermoelectric measurements, will be the focus of another publication.

The software program FullProf[21] was used for structural refinements of the NPD patterns. Peak shapes were modeled with the Thompson-Cox-Hastings pseudo-Voigt function with axial divergence asymmetry. Asymmetry parameters S/L and D/L were fixed at 0.034 and 0.035, respectively. The background for X = 8, 10, 12, and 14 was defined by a linear interpolation between a set of background points with refineable heights. The background for the X = 16 was defined by a sixth order polynomial function with origin 40° 2θ. All atoms were modeled with anisotropic thermal parameters. The number of refined parameters was 15, with typically 40 refined background points (x = 8, 10, 12, and 14). Cage volumes were calculated using a custom Java Script program.[22] Each cage was segmented into tetrahedral components, their volumes were properly summed, and the correct

dx.doi.org/10.1021/ic202095e | Inorg. Chem. 2012, 51, 1805−1812

Table 1. Site Occupancy Models[a] and Their Agreement Values (χ^2)[b] for Data Sets Collected at 35 K

	model[c] (χ^2)					bond distance model	
sample	equal %	16*i*	24*k*	6*c*/16*i*	6*c*/24*k*	χ^2	Al occupancy 24*k*, 16*i*, 6*c*
x = 8	2.374	2.393	2.419	2.353	**2.347**	**2.346**	2.13, 0.48, 5.52
x = 10	2.694	2.702	2.788	**2.648**	2.662	**2.647**	1.78, 2.40, 5.81
x = 12	2.193	2.240	2.273	2.186	**2.175**	**2.168**	1.78, 5.00, 4.75
x = 14	**2.283**	2.316	2.361	2.306	2.293	**2.273**	4.66, 5.00, 4.00
x = 15	**1.061**	1.087	1.084	1.102	1.079	**1.061**	8.22, 4.50, 2.00

[a]Al occupancy for the bond distance model is provided. [b]The values indicated in bold are the lowest values for the five models. [c]Model names and descriptions: equal %, each site contains an equal percentage of the total Al; 16*i*, all Al occupies the 16*i* site; 24*k*, all Al occupies the 24*k* site; 6*c*/16*i*, Al fully occupies the 6*c* site, and the remaining Al occupies the 16*i* site; 6*c*/24*k*, Al fully occupies the 6*c* site, and the remaining Al occupies the 24*k* site; and bond distance model, Al occupancies reflect changes in distances between Wyckoff sites (Supporting Information).

Table 2. Differences[a] in Bond Distances between Wyckoff Sites for $Ba_8Al_xSi_{46-x}$ as a Function of Increasing Al Content x and the Corresponding Expected Increase in Site Occupancy Based on the Site Connectivity

	16*i*–16*i*[a]	16*i*–24*k*[a]	24*k*–24*k*[a]	24*k*–6*c*[a]	sites which increase in Al (**necessary** and *possible*)[b]
8 → 10	*−0.0002(37)*	**0.0187(37)**	*0.0029(54)*	*−0.0001(43)*	*16i*, *24k*
10 → 12	**0.0127(38)**	**0.0125(38)**	*0.0023(64)*	*0.0044(45)*	***16i***, *24k*
12 → 14	*−0.0017(40)*	**0.0066(39)**	**0.0302(64)**	**0.0050(45)**	***24k***, *16i*, *6c*
14 → 15	**−0.0056(42)**	**0.0066(40)**	**0.0131(64)**	*−0.0004(45)*	***24k***, *16i*

[a]Differences larger than their uncertainties are given in bold; differences smaller than their uncertainties are given in italics. [b]Sites where an increase in Al is necessary are given in bold; sites where an increase in Al is possible are given in italics.

polyhedral volume was confirmed in each case by the calculated unit cell volume (2 small cage volumes + 6 large cage volumes) equaling the measured unit cell volume.

Initially, five site occupancy models were tested; Table 1 provides the agreement values (χ^2, equivalent to goodness of fit; further information on agreement values for Rietveld refinement can be found in ref 23). The models are no site preference (equal %), all Al occupies the 16*i* site (16*i*), all Al occupies the 24*k* site (24*k*), Al fully occupies the 6*c* site and remaining Al occupies the 16*i* site (6*c*/16*i*), and Al fully occupies the 6*c* site and remaining Al occupies the 24*k* site (6*c*/24*k*). Table 1 also shows χ^2 values for the bond distance model (described in detail below), along with the Al occupancies for that model. The lowest χ^2 values of the first five models provided on the left side of Table 1 are in bold. All of the bond distance model χ^2 values are in bold, and that model is the final one presented herein.

All models gave acceptable agreement values, but no one model gives the best χ^2 values for all of the compositions. The reader is encouraged to compare χ^2 values between models (horizontally) but not between samples (vertically) because slight variances in sample scattering power have led to differences in the minimal χ^2 value obtained. The best refinement for each composition with respect to each of the five models is given in bold in Table 1. The 6*c*/24*k* and 6*c*/16*i* models give the best agreement values for $x < 14$, while for $x \geq 14$, the equal % model give the best values, although only slightly. These results suggested that the Al site occupancy changed with x in a nonsystematic fashion; therefore, another model, called the bond distance model, was developed to better account for the changes in bond distance with increasing Al content.

The bond distance model is based on the changes in distance between Wyckoff sites (Table 2) and uses the site connectivity as a guide to determine where Al substitution can take place. The agreement values, χ^2, and the site occupancies for this model are also given in Table 1. As compared to the other models, the bond distance model gives equivalent or the best agreement values for all compositions. The starting occupancies of the bond distance model at the x = 8 composition are based on the refinement of the 6*c*/24*k* model, which gave the initial best agreement value out of the initial five models tested. Small adjustments to the site occupancies were made by assuming full occupancy at the site and replacing Si with Al in small steps, typically 0.3 atoms at a time. The overall Al/Si ratio determined by electron microprobe analysis was kept constant, while for the sites (24*k*, 16*i*, or 6*c*), Al/Si ratios were adjusted. The Al/Si adjustments were made based on the initial five site occupancy models, changes in bond distance with composition (Table 2 and Figure 4), and the site connectivity (Figure 1). Typically, these stepwise adjustments in site occupancy resulted in a χ^2 changing in a parabolic "well-like" manner. The final site occupancies, called the "bond distance model", are the best χ^2 values (the bottom of the well). Further details are given below.

Differences in bond distance (given in Table 2) were used to infer changes in site occupancy. Differences indicated in bold are significantly larger than their uncertainties and therefore require additional Al, and the differences indicated in italics are smaller than their uncertainties, so are not significant. These differences represent a substitution of Al for Si at one (or both) of the two sites, which define the distance. Which sites are substituted can be determined by the site connectivity (Figure 1). In Table 2, the sites where an increase in Al occupancy due to the site connectivity is necessary (bold) and possible (italics) are noted.

Increasing x from 8 to 10 causes an increase of 0.0187(37) Å in the 16*i*–24*k* distance. As x increases to 12, the 16*i*–24*k* distance continues to increase by 0.0125(38) Å along with an increase of 0.0127(38) Å in the 16*i*–16*i* distance. From x = 12 to x = 14, a large increase [0.0302(64) Å] in the 24*k*–24*k* distance is observed, accompanied by a small increase in the 16*i*–24*k* [0.0066(39) Å] and the 24*k*–6*c* [0.0050(45) Å]. The increase of x from 14 to 15 in Al displays a significant increase in the 24*k*–24*k* length [0.0131(64) Å] along with a slight increase in the 16*i*–24*k* [0.0066(40) Å] and a slight decrease in the 16*i*–16*i* [0.0056(42) Å].

The sites for which an increase in Al is necessary and possible were used as a guide to develop the bond distance model for each composition; these were the sites where the Al/Si ratio was adjusted. The connection between changes in bond distance as a function of x for adjacent compositions and the requirements of the site connectivity are complex but important. As an example, for the x = 8 to x = 10 change, the 16*i*–24*k* distance increases significantly, but the 16*i*–16*i* or 24*k*–24*k* does not. This information provided the rationale for which site occupancies should be refined for the x = 10 composition: It was necessary to refine the Al/Si ratio on both the 16*i* and 24*k* sites to see which resulted in the best agreement value. The changes in bond distances for the x = 14 and x = 15 compounds can provide a second example of how this process was employed: the 24*k*–24*k* distance increases significantly, while the 24*k*–6*c* does not. This observation led to the conclusion that the Al content must be increasing at the 24*k* site while decreasing at the 6*c* site; an improved

dx.doi.org/10.1021/ic202095e | Inorg. Chem. 2012, 51, 1805–1812

χ^2 value validated this hypothesis. Further optimization of agreement values was accomplished by trial and error. Site occupancies within this model could be varied by ~0.3 Al atoms before the refinement resulted in higher χ^2 values. In all cases, the final χ^2 values indicated that the bond distance model was the most favorable.

RESULTS AND DISCUSSION

Unit Cell and Composition. NPD data obtained at 35 K were used for structure refinement. The samples were all determined to consist of the clathrate type I phase via Rietveld refinement, and a typical NPD Rietveld refinement for the X = 8 initial composition is given in Figure 2.

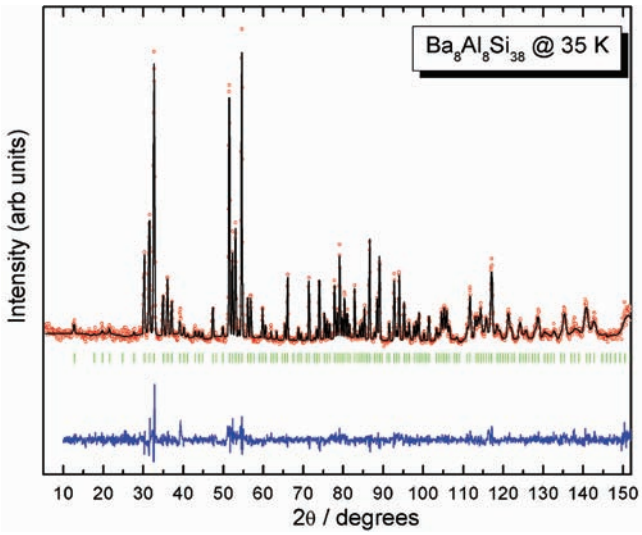

Figure 2. NPD Rietveld plot of a typical sample; $Ba_8Al_8Si_{38}$ is used in this example. Experimental data are given as red circles, the profile fit is given as a black line, *hkl* reflections for the type I phase are shown as vertical green lines, and a difference plot is given below as a blue line; λ = 1.5385 Å.

Compositional analysis, determined by electron microprobe analysis (EMPA), and lattice parameters, determined by refinement of the 35 K NPD data, are provided in Table 3. EMPA was used to determine the total Al content for each sample. Compositions determined by EPMA were similar to their starting composition, with the exception of the X = 16 initial composition, where the actual Al content is closer to x = 15. This is consistent with a recent study on the thermoelectric properties of the $Ba_8Al_xSi_{46-x}$ system,[14] where the maximum Al content of the clathrate phase was $x \sim 15$ regardless of the starting composition or annealing temperature.[13] The lattice parameters increase linearly from 10.4862(1) to 10.6213(1) Å as the Al content increases from 8.13(6) to 14.73(46). A plot of lattice parameter as a function of composition is given in Figure 3; the linear fit is the same as that recently reported for room temperature lattice parameters of $Ba_8Al_xSi_{46-x}$.[14]

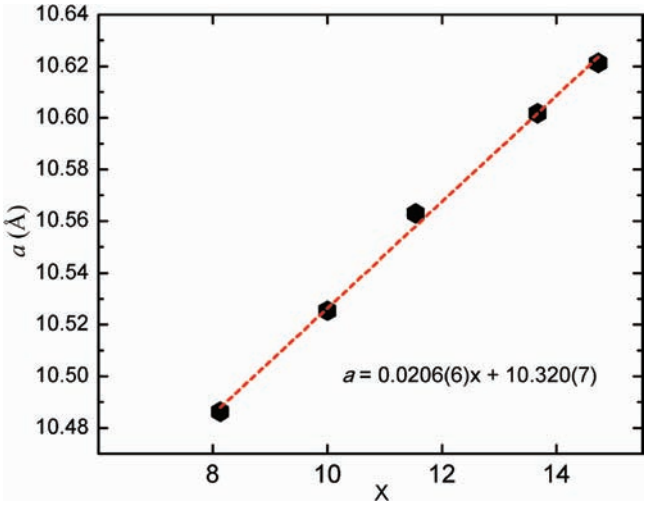

Figure 3. Lattice constant a (Å), determined by refinement of the 35 K NPD data as a function of Al content, determined by electron microprobe analysis, for $Ba_8Al_xSi_{46-x}$. The points are the data, and the red dashes indicate the linear fit: $a = 0.0206(6)x + 10.320(7)$.

Structure and Site Connectivity. The 35 K data were refined for all compositions with the type I clathrate structure (cubic space group $Pm\bar{3}n$). Various site occupancy models were refined and described in the Experimental Section; however, the bond distances were insensitive to the occupancy model used.

The covalent radius of Al (1.26 Å) is larger than Si (1.17 Å);[24] therefore, lengthening of framework bonds is expected to be correlated with substitution of Al for Si. The symmetry of the crystal structure fixes the spatial relationship between the atoms in the unit cell and thus changes in bond angles as the Al content increases are minimized. Therefore, monitoring the change in four distances between the three framework sites with increasing Al content offers insight to the site occupancy changes.

Distances between Framework Sites. Figure 4 plots the distances of the framework sites as a function of Al content x at 35 K, and Figure 5 shows the distances in the pentagons and hexagons that make up the framework. The distances are also tabulated in the Supporting Information. The 16*i*–16*i* distance is only present in the large cage, and it remains the shortest regardless of x. The 16*i*–24*k* distance is slightly larger and displays an interesting trend with increasing Al content. From x = 8 to x = 12 the 16*i*–24*k* distance steadily increases, but from x = 12 to x = 15, the rate of change is less pronounced. A similar trend is observed for the 24*k*–24*k* distances where a slight increase is observed in distances from x = 8 to x = 12, but from x = 12 to x = 15, there is a large rate of change in bond length until the 24*k*–24*k* distance becomes equal to the 24*k*–6*c* at x = 15. The 24*k*–6*c* bond is the largest in the framework and

Table 3. Electron Microprobe Composition and Lattice Parameters at 35 K for $Ba_8Al_xSi_{46-x}$

			atomic %			
initial comp. X	nominal comp.	lattice parameter (Å)	Ba	Al	Si	electron microprobe composition
8	x = 8	10.4862(1)	14.88(4)	15.05(11)	70.08(11)	$Ba_{8.04(2)}Al_{8.13(6)}Si_{37.87(6)}$
10	x = 10	10.5254(1)	14.91(3)	18.5(34)	66.59(37)	$Ba_{8.06(2)}Al_{10.00(19)}Si_{36.00(19)}$
12	x = 12	10.5630(1)	14.96(6)	21.34(7)	63.71(7)	$Ba_{8.09(4)}Al_{11.54(36)}Si_{34.46(36)}$
14	x = 14	10.6018(2)	14.94(4)	25.52(68)	59.53(67)	$Ba_{8.08(3)}Al_{13.80(36)}Si_{32.20(36)}$
16	x = 15	10.6213(1)	14.96(2)	27.25(81)	57.79(81)	$Ba_{8.10(2)}Al_{14.73(46)}Si_{31.26(44)}$

dx.doi.org/10.1021/ic202095e | Inorg. Chem. 2012, 51, 1805–1812

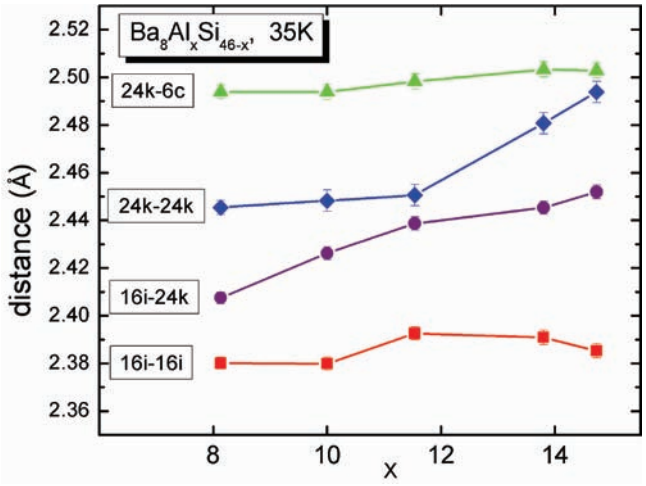

Figure 4. Distance between Wyckoff sites 6*c*, 16*i*, and 24*k* as a function of Al content, *x* (determined by electron microprobe analysis), for the four connectivities.

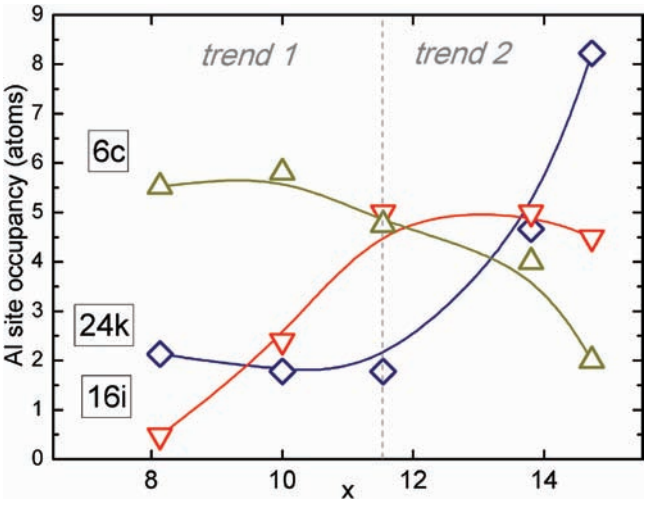

Figure 5. Al site occupancies vs *x* (total Al content determined from electron microprobe). The plot is divided into two regions: trend 1, Al occupancy of the 16*i* site increases; and trend 2, Al occupancy of the 24*k* site increases.

does not exhibit a significant dependence upon *x*. Distances that increase significantly require Al substitution, and additionally, the site connectivity dictates where the substitution can take place.

Figure 4 shows that as Al content increases, the changes in distance between sites are not increasing at a constant rate, implying a site preference. Why should there be any site preference in the structure? Site preference could be the result of two conflicting constraints: a geometric one and a chemical one. The ideal geometry for space-filling dodecahedra and tetrakaidecahedra of equal volumes has been described by Weaire and Phelan as a minimum energy[25] applicable to the macroscopic structure of foams; however, some of the computed distances between the tetrahedral sites are unreasonably short or unreasonably long, for example, 13 and 31% of the cell edge, in the context of a crystal structure. Here, the polyhedra of the type I clathrate have markedly different volumes, and the bond lengths have much less variation, so it is clear that chemical factors play a major role in determining the minimum energy structure. The Al distribution in the framework depends on the tetrahedral bond lengths and angles and the resulting cage volumes and, therefore, the distances from Ba to tetrahedral sites. All framework atoms in the type I structure are 4-coordinate; in the ideal chemical structure, the observed bond angles should be 109.5°. This is clearly not the case either, as indicated by the presence of the six-membered rings with bond angles near 120°. In the type I clathrate structure, there is a conflict between the geometric ideal vs the chemical ideal. In the case where a different atom type, such as Al, is introduced into the framework, the site at which it is placed will be that which optimizes the stability of the structure balancing both the geometric (minimize surface area) and the chemical (optimize sp^3 bond angle) ideal. The site preferences must be a consequence of this compromise. This compromise, along with the symmetry constraints of the structure, is why the bond distances do not increase at a constant rate. Understanding of the reasons for site preference is essential background for developing new type I compositions with useful properties.

Site Occupancy Refinements. The Al site occupancies as a function of *x* determined from the bond distance model are plotted in Figure 5. The plot can be divided into two sections where increasing amounts of Al localized at a specific site is observed: trend 1, Al content on the 16*i* site increases; and trend 2, Al content on 24*k* increases. The Al content at the 6*c* site gradually decreases as *x* increases. These changes are also observed in Figure 4 as an increase in the 16*i*–24*k* (trend 1) and then 24*k*–24*k* (trend 2). The increase in Al site occupancy at the 16*i* site (trend 1) serves as a good example as to why both distances and site connectivity information were required to predict the site occupancy: The site connectivity dictated that Al content could increase in either the 16*i* or the 24*k* site (or both) between *x* = 8 and 12, but refinement of a model with an increase of Al content at the 16*i* site gave better agreement values. This same process helped elucidate the decrease in Al at the 6*c* site with increasing *x*. Because there are no 6*c*–6*c* bonds, the Al content at the 6*c* site has to be inferred from changes in the 24*k*–6*c* and 24*k*–24*k* distances. Because the 24*k*-–24*k* distance shows a significant increase from *x* = 12–15 but the 24*k*–6*c* shows no significant change, the site connectivity scheme helped to determine that Al occupancy was increasing at the 24*k* site but decreasing at the 6*c* site. In summary, as Al increases in the structure, the occupancy in the 6*c*, 16*i*, and 24*k* sites decrease, increase and plateau, and increase, respectively. Improved agreement values for this model support these hypotheses concerning site occupancies.

In light of the determined site occupancy model, it is interesting to compare this model to other occupancy models for type I clathrates. Recently, X-ray and neutron single-crystal diffraction studies on the type I clathrate $Ba_8Al_{16}Ge_{30}$ were used to develop site occupancy rules, which are based on the minimization of bonds between group 13 elements.[19] The Al site occupancies obtained from the bond distances model presented herein are in good agreement with the rules when $x \leq 14$. This is not surprising because in compositions with lower Al content, bonds between Al atoms can be easily avoided. The *x* = 15 composition breaks the rule "16*i* + 24*k* sof(13) ≤ 50 %", where Al%(16*i*) + Al%(24*k*) = 28.1 + 34.3% = 62.4%. This rule can be understood by referring back to the connectivity of the 16*i* site. Because the 16*i* site is connected to three 24*k* sites, if 50% of the site were occupied by Al atoms, there should be no Al occupancy on 24*k* sites [(16 × 1/2) × 3 = 24]. However, this is somewhat misleading because each 24*k* site bridges two

dx.doi.org/10.1021/ic202095e | *Inorg. Chem.* 2012, 51, 1805–1812

16*i* sites. Therefore, if 50% of the 16*i* sites are occupied by Al atoms, eight are *not* occupied by Al atoms. Those eight sites can bridge eight 24*k* sites (or 33.3%), which could contain group 13 atoms. Therefore, the rule is better stated as 16*i* + 24*k* sof(13) ≤ 83.3%. This exception is possible because a 24*k* site bridges the 16*i* sites. No similar situation is observed for the 6*c* sites; that is, there is no 6*c*−24*k*−6*c* connectivity, and therefore, the rules hold for these cases.

Atomic Displacement Parameters. The isotropic atomic displacement parameters (*U* values) for each site are plotted versus composition (*x*) in Figure 6. Framework sites with

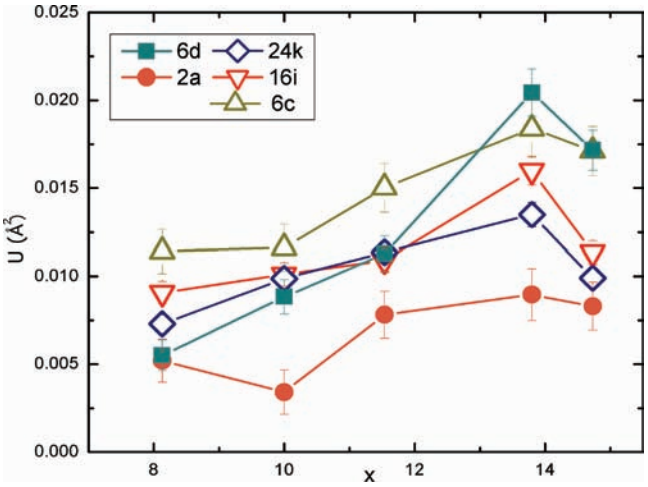

Figure 6. Isotropic atomic displacement parameters for each site with composition (*x*).

mixed occupancy tend to display larger *U* values then those without.[13,26] This is also the case here: as *x* increases, the isotropic atomic displacement parameters of the framework sites increase as well. The Ba sites display a different behavior: at *x* = 8, the *U* values for the 2*a* and 6*d* are identical, and as *x* increases, the *U* value for the 6*d* increases substantially while that for the 2*a* site does not. This difference must be attributed to positional disorder at the 6*d* site as it does not contain any mixed occupancy.

The displacement of the Ba atom in the large cage (6*d* site) has been of interest to the thermoelectric community because it may play a role in the mechanism of reducing the thermal conductivity of the material. Phases with large lattice parameters, $Ba_8Ga_{16}Ge_{30}$ (*p* type),[27] $Ba_8Ga_{16}Sn_{30}$,[28] or small cations, $Sr_8Ga_{16}Ge_{30}$,[16] $Eu_8Ga_{16}Ge_{30}$,[17] have demonstrated "glasslike" thermal conductivity. One explanation is that in these cases the large ratio of cage volume to cation size allows for a large atomic displacement at the 6*d* site. The displacement is normal to the six-membered ring at the top and bottom of the large cage and can be modeled with anisotropic displacement parameters or with a split-site model depending on the magnitude of the displacement.[17] In this study, anisotropic displacement parameters were used because the direction of displacement changes from perpendicular to the six-membered ring to parallel to it as *x* increases. Figure 7 plots the anisotropic displacement parameters with change in composition (*x*) for the 6*d* site.

Refinement of the anisotropic atomic displacement parameters at the 6*d* site results in the two displacement vectors normal to the six-membered ring being equivalent (U_{11} and U_{33}), while the U_{22} vector perpendicular to the six-membered

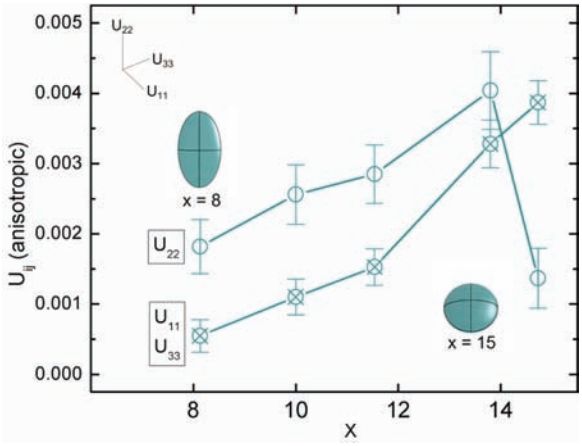

Figure 7. Anisotropic atomic displacement parameters (U_{11}, U_{22}, and U_{33}) of the 6*d* site vs composition (*x*) at 35 K. Thermal ellipsoid images of the Ba atom are shown for *x* = 8 and 15.

ring remains independent. To date, only group 13/14 phases with large displacements normal to the six-membered ring have been reported; however, this is because the phases that have been studied in most detail have *x* ∼ 16. This is not the case for the $Ba_8Al_xSi_{46-x}$ series. From *x* = 8 to 14, U_{22} is greater than $U_{11}U_{33}$, thus indicating the principal atomic displacement at the 6*d* site is perpendicular to the six-membered ring. At x = 15, $U_{11}U_{33}$ become larger, and the typical atomic displacement parallel to the six-membered ring is observed (see Figure 7). It is desirable to know if this change is due to a change in the volume of the surrounding cage or changes in the site occupancies at the sites that make up the cage.

Cage Volume. The volumes of the small and large cages in the structure have been calculated (Figure 8). Both cage

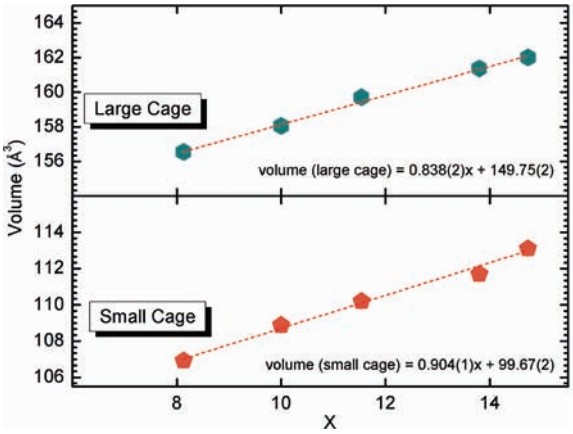

Figure 8. Cage volumes as a function of Al content of the framework at 35 K. Uncertainties were calculated based on the uncertainty in the unit cell volume; the error bars are smaller than the symbols. The red dashed lines are linear fits.

volumes increase linearly with increasing Al composition (*x*). The volume of the small cage increases from ∼107 to 113 Å^3, which can be described by a linear fit to the data: volume (small cage) = 0.904(1)*x* + 99.67(2). The volume of the large cage increases from ∼157 to 162 Å^3, which can be described by a linear fit to the data: volume (large cage) = 0.838(2)*x* + 149.75(2).

The observation that volume increases linearly with *x* is characteristic of a rigid structure or, in other words, that the

dx.doi.org/10.1021/ic202095e | Inorg. Chem. 2012, 51, 1805−1812

structure maintains its geometric angles and distances. Furthermore, this means that the observed volume changes occur due to a proportional increase in length and width of the cage, as opposed to their distortion. Linear fits to the cage volume give a larger slope for the small cage volumes, indicating that as x increases, the volume of the small cage increases at a faster rate than that of the larger cage.

Atomic Displacements as a Function of Site Occupancies and Cage Volume. It is desirable to determine if the observed changes in atomic displacement for the atom at the 6*d* site are due to an increase in volume of the cage surrounding the 6*d* site or to changes in site occupancy. This is a complex question because both cage volume and site occupancies change with composition (Figures 5 and 8). To simplify the comparison, the ratio of anisotropic atomic displacement parameters, $U_{11}U_{33}/U_{22}$, is used. Figure 9 plots the $U_{11}U_{33}/U_{22}$ ratio with cage volume.

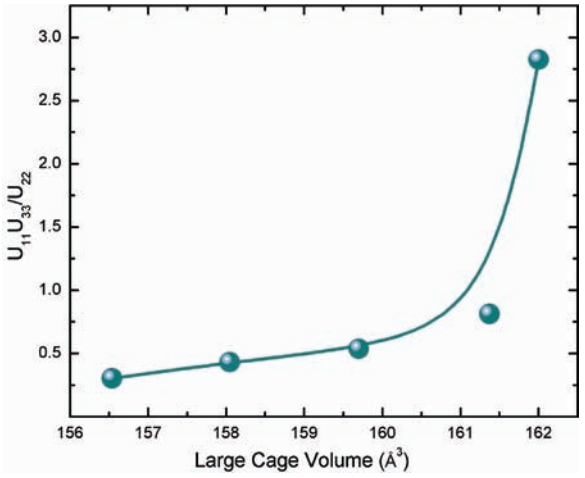

Figure 9. Ratio of atomic displacement parameter $(U_{11}U_{33})/U_{22}$ at the 6*d* site vs the large cage volume.

The $U_{11}U_{33}/U_{22}$ ratio increases as a function of large cage volume. The change in ratio is almost linear from ~157 to ~161 Å^3, which indicates that increasing cage volume increases displacement in the direction normal to the six-membered ring. When the volume becomes greater than ~161 Å^3, a sharp increase in ratio (displacement normal to the six-membered rings) is observed. This suggests that a threshold volume, ~161 Å^3, is necessary to favor atomic displacement in the direction normal to the six-membered rings; however, a contribution from the site occupancies should also be examined. To determine which of the discussed variables contributes to the atomic displacement, Figure 10 shows the plot of the large cage volume, $U_{11}U_{33}/U_{22}$ ratio, and Al site occupancy with change in composition.

The $(U_{11}U_{33})/U_{22}$ ratio increases with decreasing Al content at the 6c site and increasing Al content at the 24*k* site. Changing Al occupancy at the 16*i* site does not appear to affect the $(U_{11}U_{33})/U_{22}$ ratio. The 6*c* site is only found in the six-membered ring, while the 16*i* site is only in the circumference of the large cage, and the 24*k* site is in both locations (Figures 1 and 5). This indicates that shifting Al content from the six-membered ring, x = 8, to the circumference of the large cage, x = 15, increases atomic displacement in the direction normal to the six-membered ring. For compositions between x = 8 and x = 15, the ratio increases but never to be greater than 1. Only

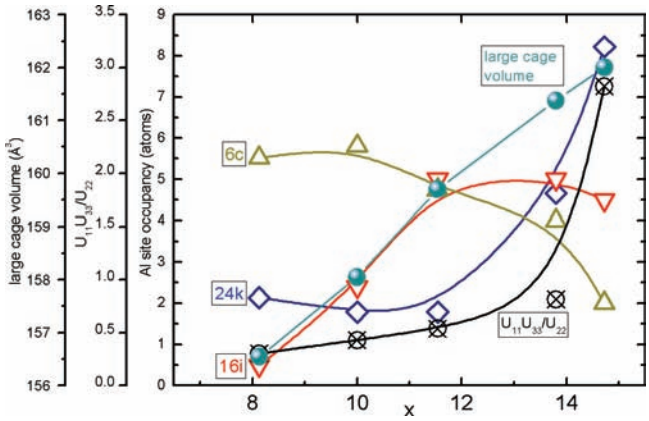

Figure 10. Plot of large cage volume (Å^3), atomic displacement parameter $(U_{11}U_{33})/U_{22}$ at the 6*d* site, and Al site occupancy vs x for $Ba_8Al_xSi_{46-x}$. Scales have been adjusted to fit all values within the plot.

when Al drops from 4 to 2 atoms at the 6*c* site, that is, when the Si content becomes greater than the Al content at the 6*c* site, does the $(U_{11}U_{33})/U_{22}$ ratio increase above 1. From a chemical standpoint, this shows that displacement of the electropositive cation at the 6*d* site is in the direction of the framework sites with the largest occupancy of electron deficient Al atoms.

To summarize, at 35 K, the change in the ratio of anisotropic displacement parameters of the atom at the 6*d* site, $(U_{11}U_{33})/U_{22}$, appears to be predominantly dependent on site occupancy of the framework. Initially, most reports[5,29] have attributed the displacement of the cation at the 6*d* site to be proportional to the volume of the cage surrounding it. The influence of the placement of group 13 atoms in the framework on displacement of the cation at the 6*d* site has been suggested in $Ba_8Ga_{16}Ge_{30}$ and $Ba_8Al_{16}Ge_{30}$, but because only one composition was studied, it was not possible to conclude this to be the case. By studying a range of compositions in the $Ba_8Al_xSi_{46-x}$ series, the connection between site occupancies and displacement of the 6*d* site is demonstrated, and thereby, the compositional dependence suggested for *n* and *p* type $Ba_8Ga_{16}Ge_{30}$ and $Ba_8Al_{16}Ge_{30}$[7,19] has validity. This is an important realization for the development of type I clathrates as thermoelectric materials as it shows that the displacement of the atom at the 6*d* site can be altered by the site occupancies of the surrounding cage.

■ CONCLUSION

The structure, site occupancies, and atomic thermal displacements of the type I clathrate $Ba_8Al_xSi_{46-x}$ have been examined as a function of composition (x) at 35 K by NPD. By observing the changes in distances between tetrahedral framework sites with increasing x, an Al/Si site occupancy model, "bond distances", was proposed and compared to other site occupancy models. The "bond distances" model gave the best agreement values.

The calculated volumes of the small and large cages increase linearly with Al content. The atomic displacement at the 6*d* site is first perpendicular to the six-membered ring in the large cage, and then, as x increases, it becomes normal to the six-membered ring. The ratio of the primary displacement parameters $(U_{11}U_{33})/U_{22}$ is used to describe this change in thermal motion at the 6*d* site and compare it to changes in cage volume and site occupancy. The Ba atomic displacements increase with increasing cage size but appear to be primarily

dx.doi.org/10.1021/ic202095e | *Inorg. Chem.* 2012, 51, 1805–1812

dependent on the framework site occupancies, specifically that displacement increases in the direction of framework sites with the largest Al content. Differences in the physical properties, specifically thermal conductivity, have been linked to the displacement of the atom at the 6*d* site. The findings reported herein emphasize the importance of site occupancies in the framework sites nearest to the atom at the 6*d* site. This correlation may better define the search for new clathrates phases with improved physical properties.

■ ASSOCIATED CONTENT

Supporting Information

Rietveld refinement fits and PXRD patterns for the $Ba_8Al_xSi_{46-x}$, where x = 10, 12, 14, and 15, and a table of distances between Wyckoff sites. This material is available free of charge via the Internet at http://pubs.acs.org.

■ AUTHOR INFORMATION

Corresponding Author

*E-mail: smkauzlarich@ucdavis.edu.

■ ACKNOWLEDGMENTS

Research at Oak Ridge National Laboratory's High Flux Isotope Reactor was sponsored by the Scientific User Facilities Division, Office of Basic Energy Sciences, U.S. Department of Energy. This work was funded by NSF Grants DMR 0600742 and DMR 1100313.

■ REFERENCES

(1) Kawaji, H.; Horie, H.; Yamanaka, S.; Ishikawa, M. *Phys. Rev. Lett.* **1995**, *74*, 1427−1429.
(2) Neiner, D.; Okamoto, N. L.; Condron, C. L.; Ramasse, Q. M.; Yu, P.; Browning, N. D.; Kauzlarich, S. M. *J. Am. Chem. Soc.* **2007**, *129*, 13857−13862.
(3) Shi, X.; Yang, J.; Bai, S. Q.; Yang, J. H.; Wang, H.; Chi, M. F.; Salvador, J. R.; Zhang, W. Q.; Chen, L. D.; Wong-Ng, W. *Adv. Funct. Mater.* **2010**, *20*, 755−763.
(4) Saramat, A.; Svensson, G.; Palmqvist, A. E. C.; Stiewe, C.; Mueller, E.; Platzek, D.; Williams, S. G. K.; Rowe, D. M.; Bryan, J. D.; Stucky, G. D. *J. Appl. Phys.* **2006**, *99*, 023708.
(5) Sales, B. C.; Chakoumakos, B. C.; Jin, R.; Thompson, J. R.; Mandrus, D. *Phys. Rev. B* **2001**, *63*, 245113.
(6) Bryan, J. D.; Blake, N. P.; Metiu, H.; Stucky, G. D.; Iversen, B. B.; Poulsen, R. D.; Bentien, A. *J. Appl. Phys.* **2002**, *92*, 7281−7290.
(7) Bentien, A.; Christensen, M.; Bryan, J. D.; Sanchez, A.; Paschen, S.; Steglich, F.; Stucky, G. D.; Iversen, B. B. *Phys. Rev. B* **2004**, *69*, 045107.
(8) Avila, M. A.; Suekuni, K.; Umeo, K.; Takabatake, T. *Phys. B-Condens. Matter* **2006**, *383*, 124−125.
(9) Toberer, E. S.; Christensen, M.; Iversen, B. B.; Snyder, G. J. *Phys. Rev. B* **2008**, *77*, 075203.
(10) Saramat, A.; Toberer, E. S.; May, A. F.; Snyder, G. J. *J. Electron. Mater.* **2009**, *38*, 1423−1426.
(11) Cederkrantz, D.; Saramat, A.; Snyder, G. J.; Palmqvist, A. E. C. *J. Appl. Phys.* **2009**, *106*, 074509.
(12) Condron, C. L.; Martin, J.; Nolas, G. S.; Piccoli, P. M. B.; Schultz, A. J.; Kauzlarich, S. M. *Inorg. Chem.* **2006**, *45*, 9381−9386.
(13) Roudebush, J. H.; Toberer, E. S.; Hope, H.; Jeffrey Snyder, G.; Kauzlarich, S. M. *J. Solid State Chem.* **2011**, *184*, 1176−1185.
(14) Tsujii, N.; Roudebush, J. H.; Zevalkink, A.; Cox-Uvarov, C. A.; Jeffery Snyder, G.; Kauzlarich, S. M. *J. Solid State Chem.* **2011**, *184*, 1293−1303.
(15) Jaussaud, N.; Gravereau, P.; Pechev, S.; Chevalier, B.; Ménétrier, M.; Dordor, P.; Decourt, R.; Goglio, G.; Cros, C.; Pouchard, M. *C. R. Chim.* **2005**, *8*, 39−46.
(16) Chakoumakos, B. C.; Sales, B. C.; Mandrus, D. G.; Nolas, G. S. *J. Alloys Compd.* **2000**, *296*, 80−86.
(17) Chakoumakos, B. C.; Sales, B. C.; Mandrus, D. G. *J. Alloys Compd.* **2001**, *322*, 127−134.
(18) Suekuni, K.; Takasu, Y.; Hasegawa, T.; Ogita, N.; Udagawa, M.; Avila, M. A.; Takabatake, T. *Phys. Rev. B* **2010**, *81*, 205207.
(19) Christensen, M.; Iversen, B. B. *Chem. Mater.* **2007**, *19*, 4896−4905.
(20) *Neutron News* **1992**, *3*, 29−37.
(21) Rodriguezcarvajal, J. *Phys. B-Condens. Matter* **1993**, *192*, 55−69.
(22) Chakoumakos, B. C.; Chakoumakos, R. M. A. Type-I clathrate cage volume calculator, unpublished.
(23) McCusker, L. B.; Von Dreele, R. B.; Cox, D. E.; Louer, D.; Scardi, P. *J. Appl. Crystallogr.* **1999**, *32*, 36−50.
(24) Sanderson, R. T. *J. Am. Chem. Soc.* **1983**, *105*, 2259−2261.
(25) Weaire, D.; Phelan, R. *Philos. Mag. Lett.* **1994**, *69*, 107−110.
(26) Jung, W.; Loerincz, J.; Ramlau, R.; Borrmann, H.; Prots, Y.; Haarmann, F.; Schnelle, W.; Burkhardt, U.; Baitinger, M.; Grin, Y. *Angew. Chem., Int. Ed.* **2007**, *46*, 6725−6728.
(27) Christensen, M.; Lock, N.; Overgaard, J.; Iversen, B. B. *J. Am. Chem. Soc.* **2006**, *128*, 15657−15665.
(28) Suekuni, K.; Tanaka, T.; Yamamoto, S.; Avila, M. A.; Umeo, K.; Takasu, Y.; Hasegawa, T.; Ogita, N.; Udagawa, M.; Takabatake, T. *J. Electron. Mater.* **2009**, *38*, 1516−1520.
(29) Nolas, G. S.; Cohn, J. L.; Slack, G. A.; Schujman, S. B. *Appl. Phys. Lett.* **1998**, *73*, 178−180.